

Associative Transformer

Yuwei Sun¹ Hideya Ochiai¹ Zhirong Wu² Stephen Lin^{*2} Ryota Kanai^{*3}

Abstract

Emerging from the pairwise attention in conventional Transformers, there is a growing interest in sparse attention mechanisms that align more closely with localized, contextual learning in the biological brain. Existing studies such as the Coordination method employ iterative cross-attention mechanisms with a bottleneck to enable the sparse association of inputs. However, these methods are parameter inefficient and fail in more complex relational reasoning tasks. To this end, we propose **Associative Transformer** (AiT) to enhance the association among sparsely attended input patches, improving parameter efficiency and performance in relational reasoning tasks. AiT leverages a learnable explicit memory, comprised of various specialized priors, with a bottleneck attention to facilitate the extraction of diverse localized features. Moreover, we propose a novel associative memory-enabled patch reconstruction with a Hopfield energy function. The extensive experiments in four image classification tasks with three different sizes of AiT demonstrate that AiT requires significantly fewer parameters and attention layers while outperforming Vision Transformers and a broad range of sparse Transformers. Additionally, AiT establishes new SOTA performance in the Sort-of-CLEVR dataset, outperforming the previous Coordination method.

1. Introduction

Transformer models use pairwise attention to establish correlations among disparate segments of input information (Vaswani et al., 2017; Dosovitskiy et al., 2020). Emerging from the pair-wise attention, there is a growing interest in leveraging sparse interactions that align more closely with the localized, contextual learning in the biological brain. This sparsity attribute has demonstrated advantages in enhancing learning performance and efficiency (Brooks, 1991;

^{*}Equal contribution ¹The University of Tokyo ²Microsoft Research ³Araya. Correspondence to: Yuwei Sun <ywsun@g.ecc.u-tokyo.ac.jp>.

Greff et al., 2020). Sparse knowledge association can find resonance with the neuroscientific grounding of the Global Workspace Theory (GWT) (Baars, 1988; Dehaene et al., 1998; VanRullen & Kanai, 2020; Juliani et al., 2022). GWT explains a fundamental cognitive architecture for working memory in the brain where diverse specialized modules compete to write information into a shared workspace through a communication bottleneck. The bottleneck facilitates the processing of content-addressable information using attention guided by contents in the shared workspace (Awh et al., 2006; Gazzaley & Nobre, 2012).

A bottleneck guides models to generalize in a manner consistent with the underlying data distribution through inductive biases of sparsity (Baxter, 2000; Goyal & Bengio, 2022), resulting in superior performance in tasks such as relational reasoning. In this regard, the Coordination method (Goyal et al., 2022) is an initial attempt to assess the effectiveness of such a bottleneck in Transformers. Unfortunately, its design is parameter inefficient and often fails in more complex relational reasoning tasks. In this work, we aim to enhance sparse attention capability by leveraging low-rank explicit memory to learn a diverse set of priors to guide the attention. Drawing inspiration from associative memory operating on Hebbian learning in the hippocampus, we utilize continuous Hopfield networks (Hopfield, 2007; Ramsauer et al., 2021) to reconstruct patches from the explicit memory. The associative memory enhances the effective association of sparsely attended historical inputs.

To this end, we propose **Associative Transformer** (AiT), a sparse representation learner augmented by associative memory. AiT learns explicit memory for each attention layer to facilitate the extraction of localized features at different abstraction levels. The explicit memory naturally evolves into specialized priors through bottleneck attention, with each focusing on a specific spatial relation for a task. We further propose a bottleneck attention balance loss to encourage diversity among the memory elements. Furthermore, the acquired priors could function as distinct attractors within the associative memory of Hopfield networks, facilitating input reconstruction from memory. Extensive empirical results demonstrate that the emerging specialization of priors and the reconstruction within associative memory could significantly enhance parameter efficiency and model performance across a broad spectrum of tasks.

Overall, the main contributions of this work are as follows:

1. We propose a novel associative memory-enhanced Transformer called the Associative Transformer (AiT). AiT tackles inefficient sparse attention in conventional Transformers by leveraging naturally emerging specialized priors for guided attention and patch reconstruction within associative memory (Section 3.3).
2. The learned priors function as attractors of Hopfield networks, facilitating information correlation and retrieval from historical inputs. To the best of our knowledge, this is the first study of leveraging Hopfield networks in the sparse attention mechanism of Transformers (Section 3.4).
3. Extensive experiments including an ablation study demonstrate enhanced performance and parameter efficiency in various image classification and relational reasoning tasks. We show that even the smallest AiT-Small model surpasses the SOTA Coordination method in the relational reasoning tasks (Section 4.2, 4.7).

2. Related Work

This section provides a summary of the most relevant recent research on sparse attention, latent memory-enabled Transformers, and external memory mechanisms. We further investigate the relatedness of these studies to the different properties of the Global Workspace Theory in Appendix B.

Sparse Transformers Studies on sparse Transformers have explored consolidating latent memory to extract localized, contextual representations from inputs (Lee et al., 2019; Gupta & Berant, 2020; Ma et al., 2021; Jaegle et al., 2021; Goyal et al., 2022; Jaegle et al., 2022). For example, Perceiver (Jaegle et al., 2021; 2022) utilized iterative cross-attention with a latent array and latent transformation to capture dependencies across input data. Set Transformer (Lee et al., 2019) and Linear Unified Nested Attention (Ma et al., 2021) also employed iterative cross-attention but without using latent transformation. Other methods, like Blockwise Self-Attention, relied on a strong assumption of predefined modularization for attention specialization (Qiu et al., 2020). In contrast, our method learns such modularization and attention specialization through end-to-end training. Unlike the vast majority of methods that employ latent memory, our proposed method leverages both explicit memory and associative memory for increased capacity and generality.

In a similar approach to constructing sparse Transformers based on GWT, the Coordination method (Goyal et al., 2022) introduced a bottleneck into cross-attention mechanisms to encourage neural module specialization. The results indicated that the competition via the bottleneck could contribute to a small set of specialized priors in latent mem-

ory to facilitate relational learning. However, the number of priors was limited to fewer than 10, all with the same dimension as the input representation. The evaluation was also restricted to simple tasks like the Triangle dataset. On the contrary, our method employs low-rank explicit memory to learn a significantly larger and richer set of priors (up to 128 priors learned from a pool of 32.8k patches). Importantly, the Coordination method relies on iterative cross-attentions, while our work focuses on a novel learning method of associative memory-enabled sparse attention.

This work is also related to modular neural networks and mixture of experts (Zuo et al., 2022; Allingham et al., 2022) in terms of competition in the shared workspace. Separating the information processing within Transformers into distinct components, depending on the input, has shown advantages in adding more flexibility in data processing.

Memory Mechanisms External memory such as tape storage and associative memory, has been employed in deep neural networks (Graves et al., 2014; Krotov & Hopfield, 2016; Gürçehre et al., 2018), with recent studies exploring the potential use of Hopfield networks and their modern variants (Hopfield, 2007; Demircigil et al., 2017; Ramsauer et al., 2021). In this work, we incorporate Hopfield networks as an integral element in the sparse attention mechanism of the proposed Associative Transformer. This approach is fundamentally different from the previous studies such as Energy Transformer (Hoover et al., 2023) that mainly focused on utilizing Hopfield networks independently of the attention mechanism.

3. Associative Transformer

This section discusses the essential building blocks of Associative Transformer (AiT), where we devise an associative memory-enabled attention layer called the *Global Workspace Layer* (GWL). The GWL comprises the low-rank explicit memory, the bottleneck attention, and the associative memory based on Hopfield networks (Figure 1).

3.1. Vision Transformers for Classification Tasks

Vision Transformers (ViT) tackle image classification tasks by processing sequences of image patches. The pre-processing layer partitions an image into non-overlapping patches. Let $x \in \mathbb{R}^{H \times W \times C}$ be an input from X , where (H, W) is the resolution of the image and C is the number of channels. x is separated into a sequence of patches $x_p \in \mathbb{R}^{N \times (P^2 \cdot C)}$, where (P, P) is the resolution of each image patch and $N = \frac{HW}{P^2}$ is the number of patches. These patches are mapped to embeddings $v_p \in \mathbb{R}^{N \times E}$ with the linear projection. ViT leverages self-attention to map a query and a set of key-value pairs to an output. The patch embeddings are used to obtain the query,

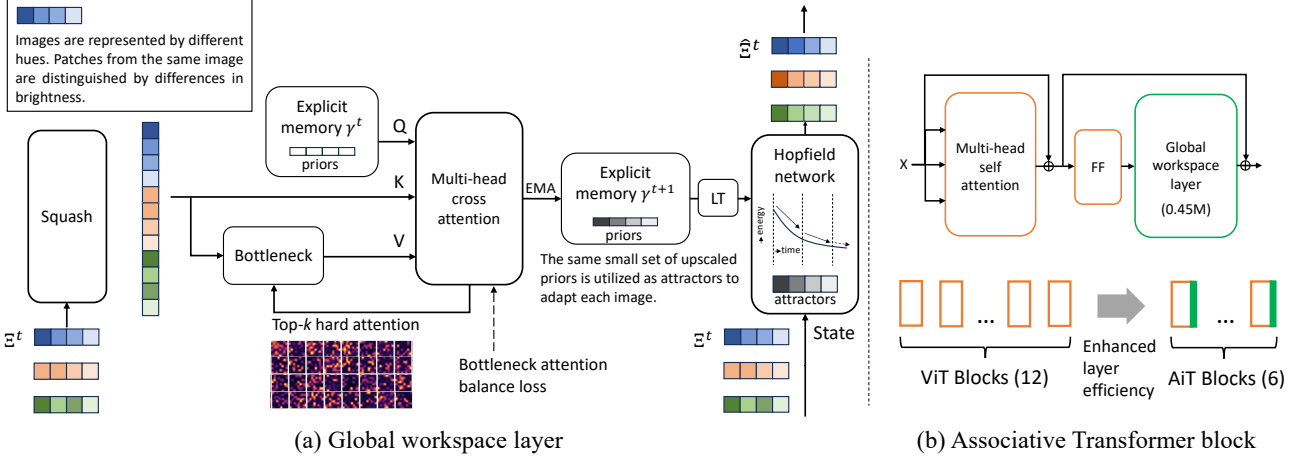


Figure 1: The scheme of the Associative Transformer (AiT). (a) In a global workspace layer, the input $\mathbb{R}^{B \times N \times E}$ is squashed into vectors $\mathbb{R}^{(B \times N) \times E}$. The squashed representations are projected to a latent space of dimension $D \ll E$ and are sparsely selected to update the explicit memory via a fixed bottleneck $k \ll (B \times N)$. The Hopfield network utilizes the memory to reconstruct the input, where a learnable linear transformation (LT) scales the memory contents back to the input dimension E . (b) The Associative Transformer block consists of self attention, feed-forward layers, and the global workspace layer. Compared to Vision Transformer (ViT), leveraging the global workspace layer enhances the layer efficiency of the model. A shallower 6-layer AiT is shown to outperform a 12-layer ViT in Table 1.

key, and value based on linear transformations $W^Q \in \mathbb{R}^{E \times D}$, $W^K \in \mathbb{R}^{E \times D}$, and, $W^V \in \mathbb{R}^{E \times D}$. The output of an individual attention head is a weighted sum of the values, $\text{softmax}\left(\frac{W_i^Q v (W_i^K v)^T}{\sqrt{D}}\right) W_i^V v$.

We specifically consider supervised learning with F categories. Let $y \in \{1, 2, \dots, F\} = Y$ denote a label. Given a Transformer model $f(x)$, the prediction is given by $\hat{y} = \arg \max_j f(x)_j$ where $f(x)_j$ denotes the j th element of $f(x)$. The training is attained by minimizing the loss with respect to the model parameter θ :

$$\ell_{\text{class}}(\theta) = J(Y, f(X; \theta)), \quad (1)$$

where J denotes the cross entropy loss.

3.2. Low-Rank Priors in Explicit Memory

The Global Workspace Layer enables an efficient writing and reading mechanism in explicit memory. The writing operation allows the explicit memory to learn a set of low-rank priors from different input patches through cross-attention. In particular, we employ a squash layer to concatenate patch representations within the entire batch $V \in \mathbb{R}^{B \times N \times E}$ into vectors $V \in \mathbb{R}^{(B \times N) \times E}$, fostering association among patches across samples. In practice, the number of patches $B \times N$ varies depending on the batch size B . However, a bottleneck with a fixed capacity k could restrict the number of attended patches to a constant value (Section 3.3).

The output of the squash layer is attended to by the multi-head cross-attention using the contents of the explicit memory as queries. The explicit memory aims to learn M low-

rank priors $\gamma = \mathbb{R}^{M \times D}$ where D is the dimension of the prior, $D \ll E$. The lower dimension is obtained through a downscaling linear transformation. We found that a rank of 32 and initialization with a Gaussian distribution works well in most cases. Priors are general assumptions about patches, such as the aggregated representations from different patches of the same attribute. The priors are used as various queries to compute cross-attentions that extract different sets of patches and update the explicit memory.

We devise a tailored cross-attention mechanism to update the explicit memory using the squash layer’s output $\Xi^t = V^t \in \mathbb{R}^{(B \times N) \times E}$. Notably, in the cross-attention, the query is a function of the current memory content $\gamma^t = \{\gamma_i^t\}_{i=1}^M$. The key and value are functions of the squashed input Ξ^t . The attention scores for head i are computed by $A_i^t(\gamma^t, \Xi^t) = \text{softmax}\left(\frac{\gamma^t W_{i,t}^Q (\Xi^t W_{i,t}^K)^T}{\sqrt{D}}\right)$. This is the case of soft attention with limited constraints on the bottleneck capacity.

3.3. Bottleneck Attention with a Limited Capacity

We discuss the case of limiting the cross-attention capacity via top- k hard attention. The hard attention constrains the number of patches that can be attended to at any given time, fostering competition among patches and ensuring the selection of the most relevant patches. Notably, we select the patches with the top- k highest attention scores from A_i^t , $\text{head}_i^t = \text{top-}k(A_i^t) \Xi^t W_i^V$. Additionally, to ensure a stable update of the explicit memory across different time steps, we employ layer normalization and the Exponentially

Weighted Moving Average (EWMA) method as follows:

$$\hat{\gamma}^t = \text{LN}(\text{Concat}(\text{head}_1^t, \dots, \text{head}_A^t)W^O), \quad (2)$$

$$\begin{aligned} \gamma^{t+1} &= (1 - \alpha) \cdot \gamma^t + \alpha \cdot \hat{\gamma}^t, \\ \gamma^{t+1} &= \frac{\gamma^{t+1}}{\sqrt{\sum_{j=1}^M (\gamma_j^{t+1})^2}}, \end{aligned} \quad (3)$$

where LN is the layer normalization and α is a smoothing factor determining the decay rate of older observations, which is usually a small value such as 0.1. EWMA ensures stable memory updates by accumulating both old γ^t and new memories $\hat{\gamma}^t$. During evaluation, we found that using different batch sizes has little influence on the test performance. This can be attributed to the small decay rate of the memory update.

Bottleneck Attention Balance Loss The sparsity induced by the bottleneck attention contributes to the emergence of specialized priors. However, cascading multiple bottleneck attentions could lead to difficulty in efficiently forming specialized priors (Figure 7). As information flows through multiple global workspace layers, the representations become diluted, necessitating a mechanism to counteract this inherent loss of input specificity. To overcome this challenge, we propose the *bottleneck attention balance loss* to encourage a more diverse selection of patches by the bottleneck attention. The bottleneck attention balance loss $\ell_{\text{bottleneck}}$ comprises two components, i.e., the accumulative attention score $\ell_{\text{importance}}$ and the chosen instances ℓ_{loads} . The loss is computed for each patch position $l \in \{1, 2, \dots, B \times N\}$ in the squash layer output. We derive the normalized variances across positions as follows:

$$\ell_{\text{importance}_{i,l}} = \sum_{j=1}^M A_{i,j,l}^t, \quad (4)$$

$$\ell_{\text{loads}_{i,l}} = \sum_{j=1}^M (A_{i,j,l}^t > 0), \quad (5)$$

$$\begin{aligned} \ell_{\text{bottleneck}_i} &= \frac{\text{Var}(\{\ell_{\text{importance}_{i,l}}\}_{l=1}^{B \times N})}{\left(\frac{1}{B \times N} \sum_{l=1}^{B \times N} \ell_{\text{importance}_{i,l}}\right)^2 + \epsilon} + \\ &\quad \frac{\text{Var}(\{\ell_{\text{loads}_{i,l}}\}_{l=1}^{B \times N})}{\left(\frac{1}{B \times N} \sum_{l=1}^{B \times N} \ell_{\text{loads}_{i,l}}\right)^2 + \epsilon}, \end{aligned} \quad (6)$$

where $A_{i,j,l}^t$ is the attention score of the position l for the j th memory slot of head i , $\text{Var}(\cdot)$ denotes the variance, and ϵ is a small value to avoid division by zero.

The losses for the different heads are summed up and added to the classification loss, $\ell = \ell_{\text{class}} + \sigma \cdot \sum_{i=1}^A \ell_{\text{bottleneck}_i}$, where σ is a coefficient to adjust the ratio between the classification loss and the bottleneck attention balance loss.

3.4. Information Retrieval with Associative Memory

After writing information into the explicit memory, the learned priors serve as attractors for a novel information retrieval component based on associative memory. The objective is to reconstruct the current input patches towards more globally meaningful representations learned and stored in the explicit memory. In particular, we employ a continuous Hopfield network to iteratively decrease the energy of a patch with respect to the learned priors in the explicit memory, enabling memory retrieval for enhanced patch representations and classification task performance. The proposed architecture is an attractor network in the sense that, in every batch, a pattern converges to one of these attractors derived from the priors stored in the explicit memory.

Attractors The learned priors in the explicit memory function as attractors within associative memory of a Hopfield network. Attractors have basins of attraction, and any input that enters an attractor's basin converges to that specific attractor. Attractors usually have the same dimension as input states. Since we employ low-rank priors γ^{t+1} , a learnable linear transformation $f_{\text{LT}}(\cdot)$ projects the priors into the same dimension E as the input before utilizing them as attractors.

Energy-Based Retrieval The upscaled priors $f_{\text{LT}}(\gamma^{t+1})$ are stored within the Hopfield network as various attractors to reconstruct the input state Ξ^t . In particular, the continuous Hopfield network employs an energy function to enable the evolution of patches into more globally meaningful representations with respect to these attractors. We update each patch representation $\xi^t \in \Xi^t$ by decreasing its energy $E(\xi^t)$ within associative memory as follows:

$$E(\xi^t) = -\text{lse}(\beta, f_{\text{LT}}(\gamma^{t+1})\xi^t) + \frac{1}{2}\xi^t \xi^{tT} + \beta^{-1} \log M + \frac{1}{2}(\max_i |f_{\text{LT}}(\gamma_i^{t+1})|)^2, \quad (7)$$

$$\hat{\xi}^t = \arg \min_{\xi^t} E(\xi^t), \quad (8)$$

where t is the batch time step, β is an inverse temperature variable, lse is the log-sum-exp function, and $\max_i |f_{\text{LT}}(\gamma_i^{t+1})|$ denotes the largest norm of attractors. In addition, a skip connection is employed to obtain the final output $\Xi^{t+1} = \hat{\Xi}^t + \Xi^t$. Although Equation 7 can be applied several times within each batch time step, we apply just a *single iteration* for each time step to ensure efficient forward and backward computation during end-to-end training. All patches reach their minimum at the same time and the global energy is guaranteed to decrease. We conducted a comparison in terms of FLOPs for the Hopfield network component in Section 4.3. Moreover, depending on β , the reconstructed input $\hat{\Xi}^t$ can be either a metastable state representing a mixture of attractors or a fixed state represented by one of the attractors. We discuss the tuning of β and further analysis of Hopfield networks in Appendix F.

4. Experiments

In this section, we present the settings and extensive empirical results for image classification tasks, including Triangle, CIFAR, and Oxford Pet, as well as the relational reasoning tasks of Sort-of-CLEVR. We conduct comprehensive ablation studies on AiT and investigate different memory initialization methods. Moreover, we demonstrate the efficacy of the bottleneck attention balance loss by visualizing the emergent prior specialization in the explicit memory.

4.1. Settings

Datasets We evaluate model performance on three different sets of datasets: (1) small classification tasks (Triangle (Goyal et al., 2022), CIFAR10, and CIFAR100 (Krizhevsky & Hinton, 2009)), (2) mid-sized classification tasks (Oxford Pet (Parkhi et al., 2012)), and (3) relational reasoning tasks (Sort-of-CLEVR (Santoro et al., 2017)). We train the model on these datasets *from scratch* using the training split and evaluate using the test split. A detailed description of the datasets can be found in Appendix A.

Model Variants We investigate three different sizes of model configurations, i.e., Small, Medium, and Base. The Base variant setting is adapted from Vision Transformer (ViT) using 12 layers, 12 attention heads for each layer, a hidden dimension of 768, and an MLP dimension of 3072. The Medium variant has 6 layers, and the Small variant has 2 layers. In what follows, we use brief notation to indicate the model size, for instance, AiT-B means the “Base” variant of the Associative Transformer. Note that the Global Workspace Layer is a light-weight attention layer with only 0.45M parameters. Further details on the various model sizes of these variants are presented in Section 4.2.

Hyperparameters *The model was evaluated with a test batch size of one. The explicit memory is only trainable during training and frozen during the evaluation.* The hyperparameters were chosen based on a grid search. A batch size of 512 was employed for the CIFAR datasets and the Triangle dataset, 128 for the Pet dataset, and 64 for the Sort-of-CLEVR dataset. We utilized the AdamW optimizer with $\beta_1 = 0.9$, $\beta_2 = 0.999$, and a weight decay of 0.01. A cosine learning rate scheduler was implemented with an initial learning rate of 1e-5, a warm-up phase of 5 (15) epochs within a total of 100 (300) epochs, and a minimum learning rate set to 1e-6. The smoothing factor of the exponentially weighted moving average, the coefficient σ , and the small value ϵ in the bottleneck balance loss were set to 0.9, 1e-2, and 1e-10, respectively. The CLS token is removed while the pooled representations of the last dense layer are used since using the CLS token undermines results in vision tasks (Wang et al., 2021; Graham et al., 2021). For AiT, we employed a memory slot size of 32 and a bottleneck attention head size of 8. We used a bottleneck size of 512 for CIFAR

and Pet, 64 for Triangle, and 256 for Relational Reasoning. We used 32 memory slots for CIFAR, Triangle, and Relational Reasoning, and 128 slots for Pet. Unless otherwise noted, we trained the model for 100 epochs and reported the mean of three individual experiments. All experiments were based on PyTorch and four A100 GPUs, and the code will be made publicly available. Please refer to Appendix C for the detailed experimental settings and hyperparameters.

4.2. Classification Tasks

The experiments on image classification tasks include comparisons to a broad range of methods. We employed the author-recommended hyperparameters to re-implement these methods. In particular, for the Coordination method, we investigated several variants with different model configurations: (1) Coordination consists of 4 layers with parameter sharing among different attention layers, (2) Coordination-D is a deeper model with 8 layers using parameter sharing, (3) Coordination-H is a high memory model with 4 layers that employ individual parameters, and (4) Coordination-DH is a high memory model with 8 layers.

The results in Table 1 demonstrate that AiT performance increased when scaling it from Small to Base, while the coordination methods could not scale with the increasing model parameter sizes. AiT also achieved better performance compared to Vision Transformers and the other sparse Transformers including Perceiver, Set Transformer, BRIMs, and Luna. Moreover, *AiT relies on significantly fewer layers and parameters while outperforming Vision Transformers*. Compared to ViT-Base using 12 layers and 85.7M parameters, AiT-Medium has only 6 layers and 45.9M parameters. Nevertheless, AiT-Medium exhibited an average performance of 81.58%, surpassing ViT-Base’s performance of 80.46%. Image classification experiments on the CIFAR and Triangle datasets demonstrate that AiT outperforms SOTA sparse Transformers and Vision Transformers, requiring a much smaller parameter size to achieve better performance.

Furthermore, we extended the evaluation to a mid-sized dataset of Oxford Pet. We trained the model from scratch for 300 epochs. Figure 2 shows that AiT-Small adds 0.9M parameters to ViT-Small while increasing the performance by 13%. Note that the proposed Global Workspace Layer is lightweight with only 0.45M parameters per attention layer. Although ViT-Base is a much larger model with 85.7M parameters and initially performed better, its accuracy quickly dropped after 50 epochs. In contrast, AiT-Medium with 45.9M parameters demonstrates a stable increase in performance and outperforms the larger ViT-Base model.

4.3. Ablation Study

A comprehensive ablation study aims to acquire insights into the functionalities of different components of AiT. In

Table 1: Performance comparison in image classification tasks.

Methods	CIFAR10 (%)	CIFAR100 (%)	Triangle (%)	Average (%)	Model Size (M)
AiT-Base	85.44	60.78	99.59	81.94	91.0
AiT-Medium	84.59	60.58	99.57	81.58	45.9
AiT-Small	83.34	56.30	99.47	79.70	15.8
Coordination (Goyal et al., 2022)	75.31	43.90	91.66	70.29	2.2
Coordination-DH	72.49	51.70	81.78	68.66	16.6
Coordination-D	74.50	40.69	86.28	67.16	2.2
Coordination-H	78.51	48.59	72.53	66.54	8.4
ViT-Base (Dosovitskiy et al., 2020)	83.82	57.92	99.63	80.46	85.7
ViT-Small	79.53	53.19	99.47	77.40	14.9
Perceiver (Jaegle et al., 2021)	82.52	52.64	96.78	77.31	44.9
Set Transformer (Lee et al., 2019)	73.42	40.19	60.31	57.97	2.2
BRIMs (Mittal et al., 2020)	60.10	31.75	58.34	50.06	4.4
Luna (Ma et al., 2021)	47.86	23.38	57.26	42.83	77.6

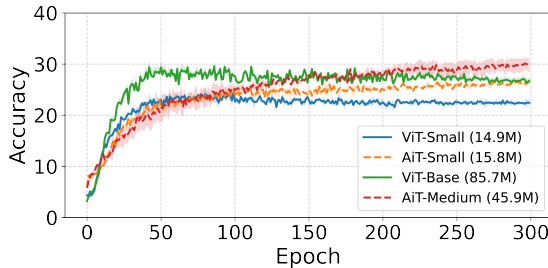


Figure 2: Comparison on the Pet dataset. AiT-Small adds 0.9M parameters to ViT-Small while increasing the performance by 13%. AiT-Medium with 45.9M parameters demonstrates a stable increase in performance and outperforms the much larger ViT-Base model.

particular, we conducted the following ablations:

- Reset Memory: The explicit memory is initialized every epoch.
- W/O Hopfield: The Hopfield network is replaced with cross-attention that shares the same architecture as the multi-head cross-attention in Figure 1.a. The cross-attention takes the input Ξ^t as the query and the upscaled priors $f_{LT}(\gamma^{t+1})$ as the key and value to compute the output $\hat{\Xi}^t = \text{MHA}(\Xi^t, f_{LT}(\gamma^{t+1}))$. The rationale behind this ablation is grounded in studies that relied on iterative cross-attentions, such as Set Transformer.
- W/O Memory: The global workspace layer is removed (equivalent to Vision Transformer).
- W/O Bottleneck: The top- k bottleneck attention is replaced with dense attention.
- W/O SA: The self-attention in Figure 1.b is removed.
- W/O FF: The feedforward network is removed.

Table 2 demonstrates that the bottleneck plays a significant role in improving performance, where its absence led to a sizable decrease in accuracy. Changes to other components,

Table 2: Comparison based on an ablation study. The results indicate that combining all the components leads to the highest performance in all the tasks.

Models	CIFAR10	CIFAR100	Triangle	Average (%)
AiT	83.34	56.30	99.47	79.70
Reset Memory	81.94	55.96	99.46	79.12
W/O Hopfield	81.03	54.96	99.44	78.48
W/O Memory	79.53	53.19	99.47	77.40
W/O Bottleneck	75.40	46.53	93.33	73.75
W/O SA	72.72	47.75	99.46	73.31
W/O FF	69.51	40.89	97.61	69.34

Table 3: FLOPs comparison for Hopfield networks.

Ablation	FLOPs
AiT	9.64×10^8
AiT with Hopfield removed	9.56×10^8
AiT with cross-attention (Hopfield replaced)	1.19×10^9

such as Hopfield networks and explicit memory, while not as impactful, still resulted in degraded accuracy. Consequently, the complete model with all the components achieved the highest accuracy.

We further conducted a comparison in terms of FLOPs for Hopfield network ablations against the baseline AiT method in Table 3. We clarify that the Hopfield network was trained using a single forward-backward iteration, making it lightweight (with less than 0.84% FLOPs increase), especially when compared to the cross attention-based method.

4.4. Parameter Efficiency Compared with Coordination

Benefits of incorporating the Global Workspace Layer include its parameter efficiency and better performance. We conducted an extensive comparison of AiT’s parameter effi-

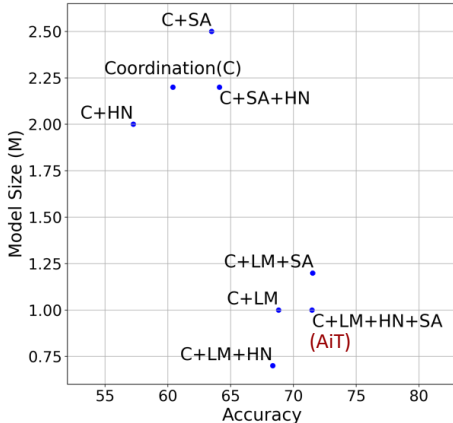


Figure 3: Model size vs. test accuracy for various configurations within a single attention block. Consolidating all the components in the Coordination block (C+LM+HN+SA), i.e., an AiT block, resulted in the best performance of 71.49% while maintaining a compact model size of 1.0M.

ciency by measuring the model size and corresponding test accuracy on the CIFAR-10 dataset. Specifically, we compared a single AiT block to a single Coordination block that consists of two connected multi-head cross-attention components. We explored various configurations by replacing one or all of the cross-attentions with the proposed components in AiT. In particular, in Figure 3, ‘C’ denotes the default Coordination block, ‘LM’ denotes the ablation replacing the first cross-attention in the Coordination block with the proposed low-rank explicit memory, ‘HN’ denotes the ablation replacing the second cross-attention with the proposed Hopfield network component, and ‘SA’ denotes the ablation using the self-attention.

Figure 3 demonstrates that *leveraging the low-rank memory (LM) can improve performance and also reduce the model parameter size*. Compared to Coordination (C) which achieved an accuracy of 60.41% with a model size of 2.2M, integrating the low-rank memory (C+LM) significantly improved accuracy while reducing the model size to 1M. Moreover, the Hopfield network (HN) based on the energy function brings improvements (C+SA+HN) or retains the model performance (C+LM+HN+SA) while reducing the parameter size. In addition, HN appeared to be effective only when the LM or SA component was applied. We assume that retrieval within the associative memory of the Hopfield network relies on a diverse set of priors, which is learned by the low-rank memory and further enhanced by the self-attention. Consequently, consolidating all three components in the Coordination block (C+LM+HN+SA), i.e., an AiT block, resulted in the best performance of 71.49% while maintaining a compact model size of 1.0M. The results demonstrate that AiT is an efficient sparse representation learner, surpassing the SOTA Coordination method in terms of both test accuracy and parameter efficiency.

Table 4: Different memory initialization approaches. The Gaussian distribution was found to give the best result.

Memory initialization methods	Accuracy (%)
Gaussian distribution	83.34
Uniform distribution (Graves et al., 2014)	81.92
Identity distribution (Goyal et al., 2022)	78.56

4.5. Explicit Memory Initialization

To initialize the explicit memory, we set each slot with values drawn from a specific distribution, including the Gaussian distribution, the uniform distribution (Graves et al., 2014), and the identity distribution (Goyal et al., 2022). In particular, the Gaussian distribution generates random values with a mean of zero and a variance of one. The uniform distribution (Graves et al., 2014) utilizes an upper bound of $\frac{1}{\sqrt{M+D}}$, where M is the memory slot number, and D is the slot size. The identity distribution (Goyal et al., 2022) assigns ones on the diagonal and zeros elsewhere. Table 4 indicates that the Gaussian distribution resulted in the best performance, which potentially prevents specific memory slots from dominating the learning process, for a more balanced memory update in the early training stages.

4.6. Prior Specialization via Bottleneck Attention Balance Loss

The Bottleneck Attention Balance Loss encourages competition among patches, facilitating the selection of diverse patches through the bottleneck. To quantitatively measure efficacy, we computed a diversity score, i.e., the ratio of distinct patches in the selected patches by all priors in the explicit memory. Figure 8 in Appendix E shows an apparent increase in the diversity of patches as training progresses.

We aim to investigate whether the bottleneck attention could contribute to specialized priors that guide attention to different localized features. To this end, for each prior in the explicit memory, we visualized its attention scores computed by Equation 2 over different patches in Figure 4, where the selected patches are highlighted. Interestingly, despite employing the squash layer to concatenate patches across different batch samples, each prior eventually learned to extract from similar patch input positions for different samples. These priors demonstrated emergent specialization, focusing on specific spatial areas in an image.

4.7. Relational Reasoning

The specialization of priors in the spatial allocation of attention contributes to AiT’s enhanced performance in relational reasoning tasks. The goal is to answer questions about the properties and relations of various objects based on a given image. AiT leverages different priors to facil-

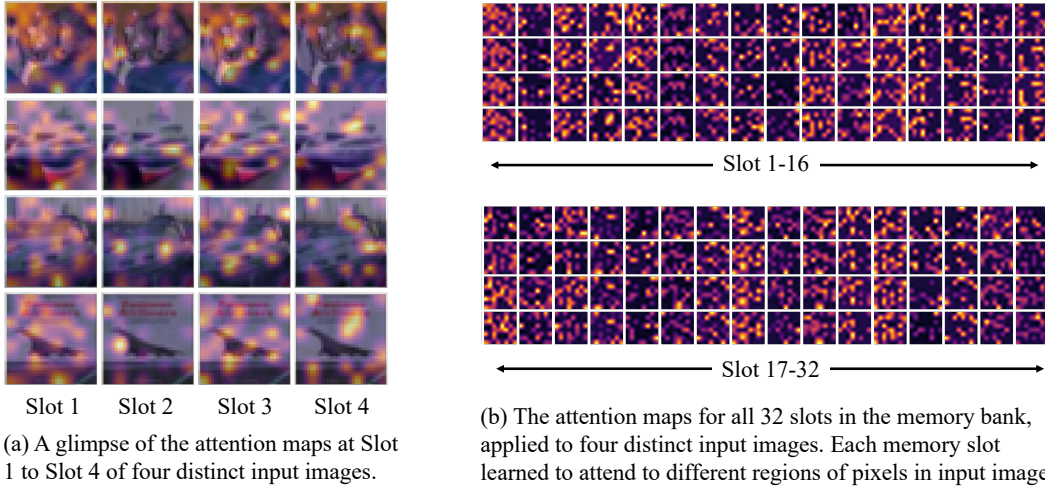


Figure 4: Prior-guided attention visualization highlights selected patches, with each prior having learned to extract from similar patch input positions across different samples. These priors exhibit emergent specialization, focusing on specific spatial areas in an image (using the first global workspace layer of AiT-Small in CIFAR-10).

Table 5: Relational reasoning task performance.

Methods	Relational Non-relational(%)	
Transformer based models		
AiT-Base	80.03	99.98
AiT-Small	76.82	99.85
Coordination (Goyal et al., 2022)	73.43	96.31
Set Transformer (Lee et al., 2019)	47.63	57.65
Non-Transformer based models		
CNN+LSTM (Santoro et al., 2017)	60.08	99.47
Dense-Base	46.93	57.71
Dense-Small	47.28	57.68

itate associations among different image regions for the question-answering tasks. In particular, we evaluated AiT’s performance in the Sort-of-CLEVR dataset (Santoro et al., 2017), comprising non-relational and relational tasks. In the non-relational tasks, the question involves the attributes of a specific object, whereas in the relational tasks, the question focuses on the relations between different objects.

To tackle the Sort-of-CLEVR tasks, we embedded the question using a learnable linear projection, with layer normalization applied before and after the embedding. Then, the question embedding was concatenated to the image patch embeddings as the input to AiT. We compared AiT to both Transformer-based models including Set Transformer and Coordination, and other non-Transformer based models including CNN+LSTM (Santoro et al., 2017) and Dense networks. In CNN+LSTM, images are processed with a CNN to produce a set of objects, and questions are processed with an LSTM to generate a question embedding. Then, an MLP combines both the image and question embed-

dings to answer the question. In addition, Dense-Small and Dense-Base are two fully-connected models derived from AiT-Small and AiT-Base, respectively.

The results in Table 5 demonstrate a substantial improvement in AiT’s performance in both relational and non-relational tasks compared to existing Transformer-based methods of Coordination and Set Transformer. AiT achieved a competitive test accuracy of 80.03% in the relational reasoning tasks. The superior performance with associative memory can be attributed to the inherent sparse attention guided by the explicit memory, allowing the allocation of attention to specific areas of images for different tasks.

5. Limitations and Conclusions

We proposed the Associative Transformer (AiT) with explicit memory and Hopfield networks to enhance associations among sparsely attended input patches. AiT demonstrated largely improved parameter efficiency and performance across various classification and relational reasoning tasks, surpassing Vision Transformers and conventional sparse Transformers. AiT also established a new SOTA performance in the Sort-of-CLEVR dataset, outperforming the Coordination method.

While AiT demonstrates considerable capability, scaling it to larger dataset training without fine-tuning hyperparameters such as the inverse temperature and bottleneck size, remains a challenge. Overall, we are excited about introducing localized contextual learning and associative memory into Transformers by focusing on diverse rather than narrow patch representation learning and selection for tasks involving classification and relational reasoning.

References

- Allingham, J. U., Wenzel, F., Mariet, Z. E., and et al. Sparse moes meet efficient ensembles. *Transactions on Machine Learning Research*, 2022. 2
- Awh, E., Vogel, E. K., and Oh, S.-H. Interactions between attention and working memory. *Neuroscience*, 139(1): 201–208, 2006. 1
- Baars, B. J. *A Cognitive Theory of Consciousness*. Cambridge University Press, 1988. 1
- Baxter, J. A model of inductive bias learning. *Journal of artificial intelligence research*, 12:149–198, 2000. 1
- Brooks, R. A. Intelligence without representation. *Artif. Intell.*, 47(1-3):139–159, 1991. 1
- Dehaene, S., Kerszberg, M., and Changeux, J. A neuronal model of a global workspace in effortful cognitive tasks. *Proceedings of the National Academy of Sciences*, 95(24): 14529–14534, 1998. 1
- Demircigil, M., Heusel, J., L’owe, M., Upgang, S., and Vermet, F. On a model of associative memory with huge storage capacity. *Journal of Statistical Physics*, 168(2): 288–299, 2017. 2
- Dosovitskiy, A., Beyer, L., Kolesnikov, A., Weissenborn, D., Zhai, X., Unterthiner, T., Dehghani, M., Minderer, M., Heigold, G., Gelly, S., et al. An image is worth 16x16 words: Transformers for image recognition at scale. *arXiv preprint arXiv:2010.11929*, 2020. 1, 6, 11
- Gazzaley, A. and Nobre, A. C. Top-down modulation: bridging selective attention and working memory. *Trends in cognitive sciences*, 16(2):129–135, 2012. 1
- Goyal, A. and Bengio, Y. Inductive biases for deep learning of higher-level cognition. *Proceedings of the Royal Society A*, 478(2266):20210068, 2022. 1
- Goyal, A., Didolkar, A. R., Lamb, A., and et al. Coordination among neural modules through a shared global workspace. In *ICLR*, 2022. 1, 2, 5, 6, 7, 8, 11
- Graham, B., El-Nouby, A., Touvron, H., and et al. Levit: a vision transformer in convnet’s clothing for faster inference. In *ICCV*, pp. 12239–12249, 2021. 5
- Graves, A., Wayne, G., and Danihelka, I. Neural turing machines. *arXiv preprint arXiv:1410.5401*, 2014. 2, 7
- Greff, K., van Steenkiste, S., and Schmidhuber, J. On the binding problem in artificial neural networks. *arXiv preprint arXiv:2012.05208*, 2020. 1
- Gülçehre, Ç., Chandar, S., Cho, K., and Bengio, Y. Dynamic neural turing machine with continuous and discrete addressing schemes. *Neural Comput.*, 30(4), 2018. 2
- Gupta, A. and Berant, J. GMAT: global memory augmentation for transformers. *arXiv preprint arXiv:2006.03274*, 2020. 2, 11
- Hoover, B., Liang, Y., Pham, B., and et al. Energy transformer. *arXiv preprint arXiv:2302.07253*, 2023. 2
- Hopfield, J. J. Hopfield network. *Scholarpedia*, 2(5):1977, 2007. 1, 2
- Jaegle, A., Gimeno, F., Brock, A., and et al. Perceiver: General perception with iterative attention. In *ICML*, volume 139 of *Proceedings of Machine Learning Research*, pp. 4651–4664. PMLR, 2021. 2, 6, 11
- Jaegle, A., Borgeaud, S., Alayrac, J., and et al. Perceiver IO: A general architecture for structured inputs & outputs. In *ICLR*, 2022. 2, 11
- Johnson, J., Hariharan, B., van der Maaten, L., and et al. CLEVR: A diagnostic dataset for compositional language and elementary visual reasoning. In *CVPR*, pp. 1988–1997, 2017. 11
- Juliani, A., Arulkumaran, K., Sasai, S., and Kanai, R. On the link between conscious function and general intelligence in humans and machines. *Transactions on Machine Learning Research*, 2022. 1
- Krizhevsky, A. and Hinton, G. Learning multiple layers of features from tiny images. Technical report, 2009. 5, 11
- Krotov, D. and Hopfield, J. J. Dense associative memory for pattern recognition. In *NIPS*, pp. 1172–1180, 2016. 2
- Lee, J., Lee, Y., Kim, J., and et al. Set transformer: A framework for attention-based permutation-invariant neural networks. In *ICML*, pp. 3744–3753, 2019. 2, 6, 8, 11
- Ma, X., Kong, X., Wang, S., and et al. Luna: Linear unified nested attention. In *NeurIPS*, pp. 2441–2453, 2021. 2, 6, 11
- Mittal, S., Lamb, A., Goyal, A., Voleti, V., Shanahan, M., Lajoie, G., Mozer, M., and Bengio, Y. Learning to combine top-down and bottom-up signals in recurrent neural networks with attention over modules. In *International Conference on Machine Learning*, pp. 6972–6986. PMLR, 2020. 6, 11
- Parkhi, O. M., Vedaldi, A., Zisserman, A., and Jawahar, C. V. Cats and dogs. In *CVPR*, pp. 3498–3505, 2012. 5, 11

Qiu, J., Ma, H., Levy, O., and et al. Blockwise self-attention for long document understanding. In *EMNLP (Findings)*, pp. 2555–2565, 2020. [2](#), [11](#)

Ramsauer, H., Schäfl, B., Lehner, J., and et al. Hopfield networks is all you need. In *ICLR*, 2021. [1](#), [2](#), [11](#), [13](#)

Santoro, A., Raposo, D., Barrett, D. G. T., and et al. A simple neural network module for relational reasoning. In *NIPS*, pp. 4967–4976, 2017. [5](#), [8](#), [11](#)

VanRullen, R. and Kanai, R. Deep learning and the global workspace theory. *arXiv preprint arXiv:2012.10390*, 2020. [1](#)

Vaswani, A., Shazeer, N., Parmar, N., and et al. Attention is all you need. *NeurIPS*, pp. 5998–6008, 2017. [1](#)

Wang, W., Xie, E., Li, X., and et al. Pyramid vision transformer: A versatile backbone for dense prediction without convolutions. In *ICCV*, pp. 548–558, 2021. [5](#)

Zuo, S., Liu, X., Jiao, J., and et al. Taming sparsely activated transformer with stochastic experts. In *ICLR*, 2022. [2](#)

A. Datasets

In this section, we describe the datasets used in this work. (1) CIFAR-10 is an image collection of 10 objects, covering 50k training samples and 10k test samples, labeled as airplane, automobile, and so on. The size of images is $32 \times 32 \times 3$. (2) CIFAR-100 (Krizhevsky & Hinton, 2009) contains 100 object classes with 500 training images and 100 testing images per class. For both the CIFAR-10 and CIFAR-100 datasets, we performed random cropping with size $32 \times 32 \times 3$ and a padding size of 4. (3) Triangle dataset (Goyal et al., 2022) includes 50k training images and 10k test images with size 64×64 , each of which contains 3 randomly placed clusters of points. The task is to predict whether the three clusters form an equilateral triangle or not. (4) Oxford-IIIT Pet dataset (Parkhi et al., 2012) comprises 37 categories featuring diverse breeds of cats and dogs, with 200 images allocated for each class. We utilized random resized cropping with size $256 \times 256 \times 3$ and resized all images to size $224 \times 224 \times 3$. Additionally, we applied random horizontal flip and normalization to the CIFAR-10, CIFAR-100, and Oxford-IIIT Pet datasets. (5) Sort-of-CLEVR dataset (Santoro et al., 2017) is a simplified version of the CLEVR dataset (Johnson et al., 2017). It includes 10k images with size $75 \times 75 \times 3$ and 20 different questions (10 relational and 10 non-relational questions) for each image. In each image, objects with randomly chosen shapes (square or circle) and randomly chosen colors (red, green, blue, orange, gray, yellow) are placed (Figure 5).

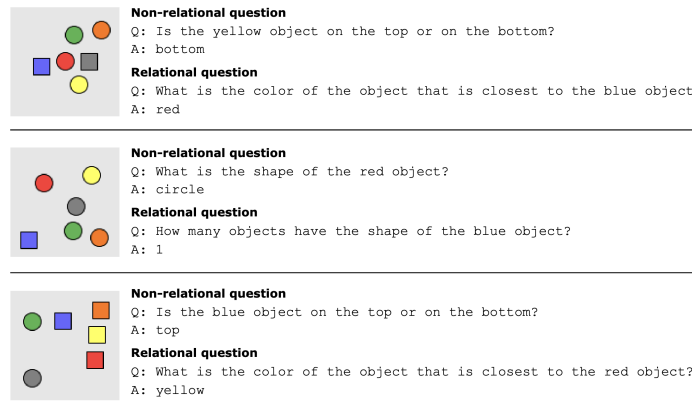


Figure 5: Examples from the Sort-of-CLEVR dataset (Santoro et al., 2017).

B. Comparison of Work Related to Global Workspace Theory

We discuss and summarize the existing sparse attention methods in relation to the properties of Global Workspace Theory (Table 6). First, we examine whether an architecture involves operations of information writing and reading through a shared workspace. Secondly, we assess whether the latent representations (priors) in workspace memory are subsequently processed by self-attention. Thirdly, we inspect whether the latent representations have a lower rank compared to the input representations. Fourthly, we analyze whether information retrieval from the workspace is driven by a bottom-up or a top-down signal. Lastly, we investigate whether the model incorporates a bottleneck with a limited capacity to regulate the information flow passing through the workspace.

Table 6: Comparison of attention architectures based on properties of the Global Workspace Theory.

Method	Operations		Self-Attention	Low-Rank Memory	Top-Down/Bottom-Up	Bottleneck
	Writing	Reading				
Vision Transformer (Dosovitskiy et al., 2020)	✗	✗	✓	✗	BU	✗
BlockBERT (Qiu et al., 2020)	✗	✗	✓	✗	BU	✓
BRIMs(Mittal et al., 2020)	✗	✗	✗	✗	TD	✓
Modern Hopfield (Ramsauer et al., 2021)	✗	✓	✗	✓	BU	✗
Perceiver (Jaegle et al., 2021)	✓	✗	✓	✓	BU	✗
Coordination (Goyal et al., 2022)	✓	✓	✗	✗	BU	✓
Perceiver IO (Jaegle et al., 2022)	✓	✓	✓	✓	TD	✗
Set Transformer (Lee et al., 2019)	✓	✓	✗	✗	BU	✗
Luna (Ma et al., 2021)	✓	✓	✗	✗	BU	✗
GMAT (Gupta & Berant, 2020)	✓	✓	✓	✗	BU	✓
Associative Transformer (Ours)	✓	✓	✓	✓	BU	✓

C. Experimental Settings and Hyperparameters

Table 7 presents the hyperparameters used for the different tasks in this study. Unless otherwise noted, we employed the author-recommended settings and hyperparameters for the re-implementation of baseline models. The small variants of ViT and AiT have 2 attention layers, and the base variants of them have 12 attention layers instead. We used the same dimension of the hidden layer and the MLP layer for ViT and AiT. By default, we employed 8 attention heads and 32 memory slots for the bottleneck attention. To obtain the bottleneck size, we considered two main factors of the batch size and the patch size. For the CIFAR and Pet datasets, we used a bottleneck size of 512, which selected from a pool of 32.8k/25.1k patches. For the Triangle dataset, we used a bottleneck size of 64 from a pool of 2.0k patches. For the relational reasoning tasks, we used a bottleneck size of 256, which selected from a pool of 14.4k patches. Based on the bottleneck size and the patch pool size, we used 128 memory slots for the Pet dataset and 32 memory slots for the other datasets. Moreover, we trained the models on the Pet dataset for 300 epochs and on the other datasets for 100 epochs. In relational reasoning tasks, we trained all models for 100 epochs with a batch size of 64.

Table 7: Hyperparameters.

Parameter	Value
Common parameters	
Optimizer	AdamW
Weight decay	0.01
Learning rate	1×10^{-4}
Number of self-attention heads	12
Number of attention layers	2 (Small)/ 12 (Base)
Size of hidden layer	768
Size of MLP	3072
Size of memory slot	32
Number of bottleneck attention heads	8
Beta	1.0
Epochs	100 (300 for Oxford Pet)
CIFAR	
Patch size	4
Batch size	512
Number of memory slots	32
Bottleneck size	512
Triangle	
Patch size	32
Batch size	512
Number of memory slots	32
Bottleneck size	64
Oxford Pet	
Patch size	16
Batch size	128
Number of memory slots	128
Bottleneck size	512
Relational reasoning	
Patch size	5
Batch size	64
Number of memory slots	32
Bottleneck size	256

D. Analysis of Attention Head Operating Modes

We assume that the competition within the pair-wise attention is important for the model to learn meaningful representations. If such competition exists, a trained model will naturally result in sparser interactions in attention heads. Therefore, we first performed an analysis of the operating modes of different attention heads in a pretrained ViT model by measuring the number of patches each head is attending to. We trained a ViT-Base variant model for 100 epochs from scratch for the CIFAR-10 task. Then, for each attention head, we obtained a violin plot to represent the distribution of attention sparsity for different patches (Figure 6). The attention sparsity for a specific patch’s interactions with other patches is computed as follows $\arg \min_s \sum_{j=1}^s A^{i,j} \geq 0.9$, where $A^{i,j}$ is the attention score allocated to the j th patch by the i th patch. The attention sparsity score is measured by the minimal number of required patches whose attention scores add up to 0.90. For instance, there are 65 patches for the CIFAR-10 task with patch size 4, thus there are 65 interactions for each patch to all the patches including itself. An attention head has a higher sparsity if the median \bar{s} of the required patches is smaller, which is the number in the center of each panel. The heads in each layer are sorted according to \bar{s} . Note that training the model for a longer duration can result in even better convergence and higher attention sparsity. We also refer to a concurrent investigation on the Bidirectional Encoder Representations from Transformers (BERT) for results on the natural language processing (NLP) tasks (Ramsauer et al., 2021).

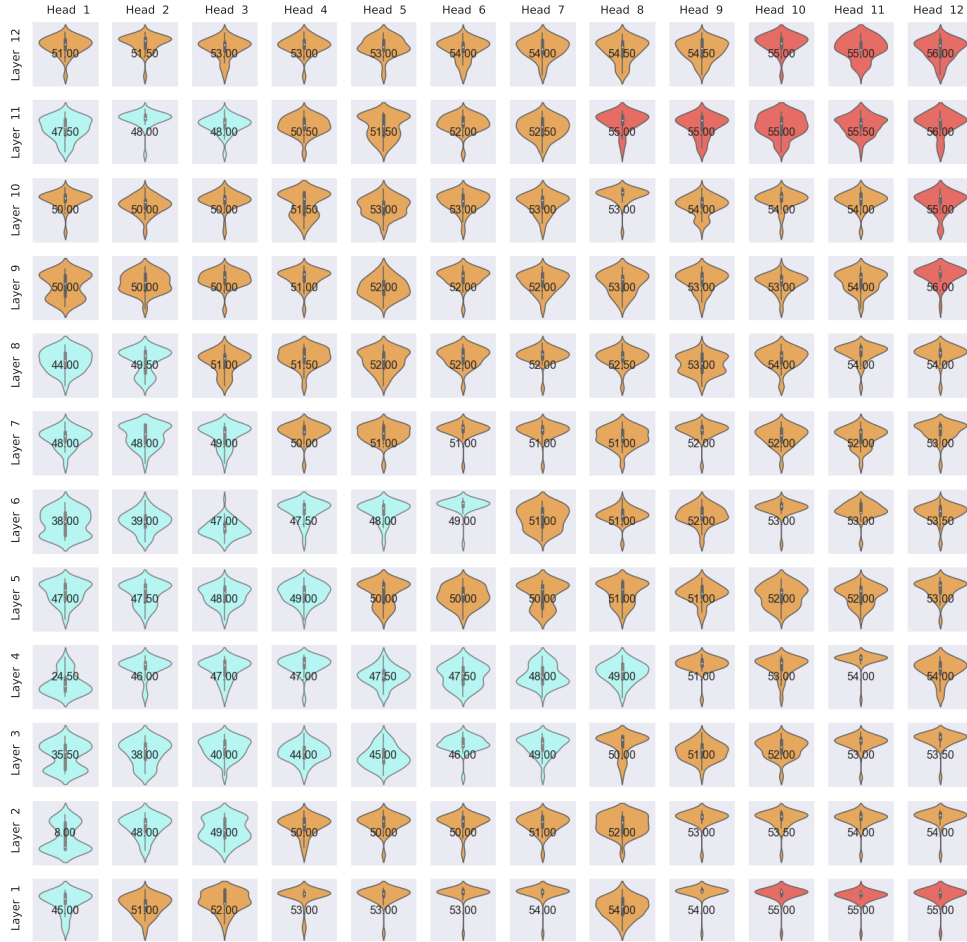


Figure 6: Analysis of operating modes of attention heads in the ViT-Base model. We recognize three different groups of attention heads based on their sparsity scores. Group (I) in light blue: High sparsity heads abundant in the middle layers 3-6. The vast majority of these heads only used 50% or fewer interactions. Group (II) in orange: Middle sparsity heads predominant in layers 2 and 7-10. Less than 80% of the interactions were activated. Group (III) in red: Low sparsity heads observed in high layers 11-12 and the first layer, where the most patches were attended to. The global workspace layer will provide the inductive bias to attend to the essential patches more effectively.

Compared to NLP tasks, much less sparsity was found in ViT models. This can be attributed to the long-range dependencies of the attention mechanism were more frequently employed in handling patches of images, compared to handling tokens in text sequences. In ViT models, an input image is divided into non-overlapping patches which are then treated as separate "tokens" and fed into the transformer model. By contrast, the sequential nature of the NLP text data allows the model to capture long-range dependencies among long-range tokens more easily.

E. Efficacy of the Bottleneck Attention Balance Loss

The Bottleneck Attention Balance Loss facilitates the learning of priors that attend to diverse sets of patches. We demonstrate the efficacy by visualizing the bottleneck attention scores (Figure 7) and the selected patches by the bottleneck attention (Figure 8). We employed as a metric for patch diversity the ratio of distinct patches in all the selected patches.

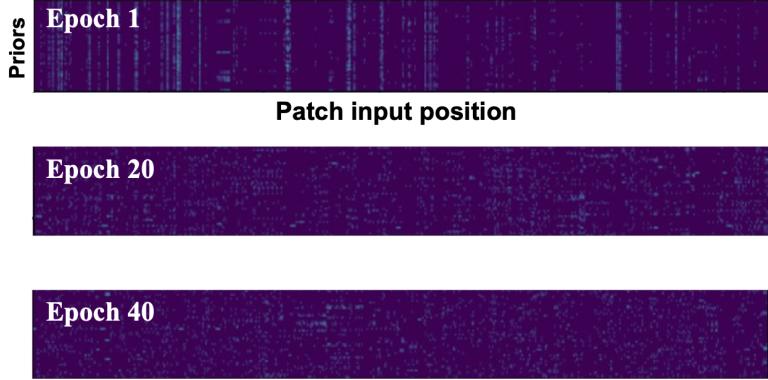


Figure 7: The Bottleneck Attention Balance Loss facilitates the selection of more diverse patches from various input positions.

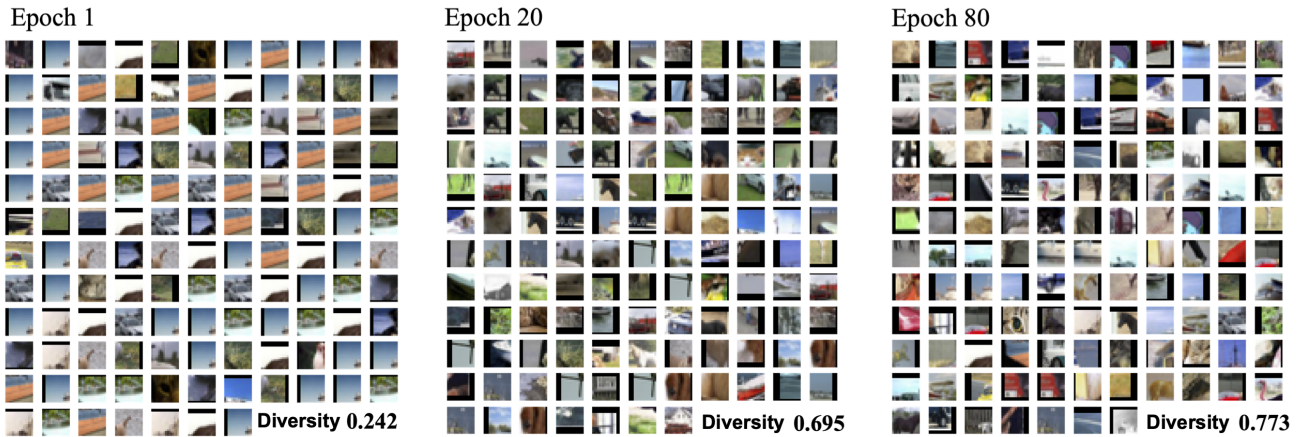


Figure 8: Selected patches by the bottleneck attention in CIFAR-10, demonstrating an apparent increase in the diversity of selected patches as training progresses.

F. Hopfield Networks Energy

In traditional Hopfield networks, it is possible to store N samples and retrieve them with partially observed or noisy patterns by updating model weights. During retrieval, these partially observed or noisy patterns converge to one of these attractors, minimizing the Hopfield energy. Unlike traditional Hopfield attractors that incorporate the implicit memory within its model parameters, AiT decouples the memory from the Hopfield network by introducing the learnable explicit memory. This memory serves the functions of both priors in the bottleneck attention and attractors in Hopfield networks. Consequently, the Hopfield network does not need to store different inner states every batch time, instead, we can reuse the learned memory

bank from the bottleneck attention to update and maintain a set of attractors with the trainable linear transformation. The proposed architecture is an attractor network in the sense that, in every batch, a pattern converges to one of these attractors derived from the priors stored in the explicit memory bank.

Moreover, the information retrieval is based on a continuous Hopfield network, where an input state converges to a fixed attractor point within the associative memory of the Hopfield network. Usually, any input state that enters an attractor's basin of attraction will converge to that attractor. The convergence results in a decreased state energy with respect to the stored attractors in the memory. All patches reach their minimum at the same time and the global energy in Equation 7 is guaranteed to decrease. To quantitatively measure the amount of energy reduction during the information retrieval process in the Hopfield network, we computed an input state's energy before and after it was reconstructed. A successful retrieval results in substantial reduction in the state energy (Figure 9).

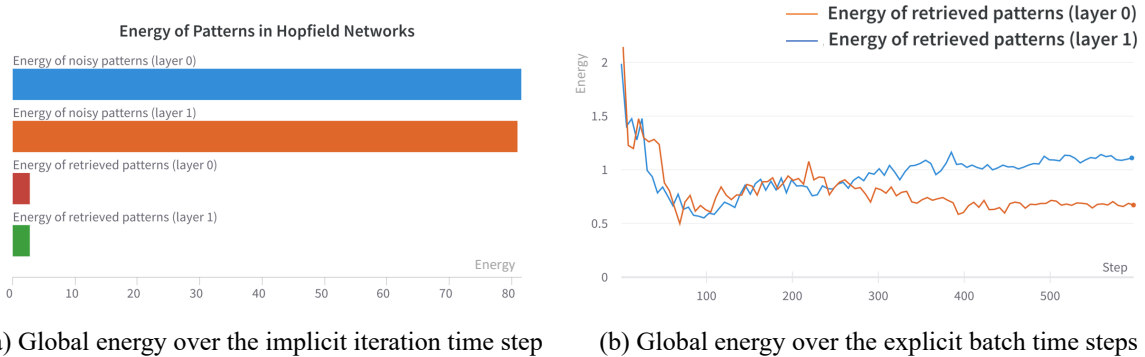


Figure 9: AiT-Small's patch representation energy for the CIFAR-10 task. The Hopfield network operates by iteratively decreasing the energy of an input state with respect to the attractors stored in its memory. This reduction in energy enables the retrieval of a representation that closely aligns with learned attractors, effectively leveraging knowledge within the associative memory. The energy is guaranteed to decrease over the iteration time step for every retrieval. Over the batch time steps, the energy generally decreases, especially during the early stages of training.

Furthermore, we investigated the effect of the inverse temperature β on the information retrieval capability of Hopfield networks in Figure 10. We found that using an inverse temperature of 1.0 obtained the best retrieval performance based on the Hopfield networks. The results suggest that the inverse temperature parameter requires tuning to reach optimal performance. We aim to study a mechanism to adjust β adaptively in a future study.

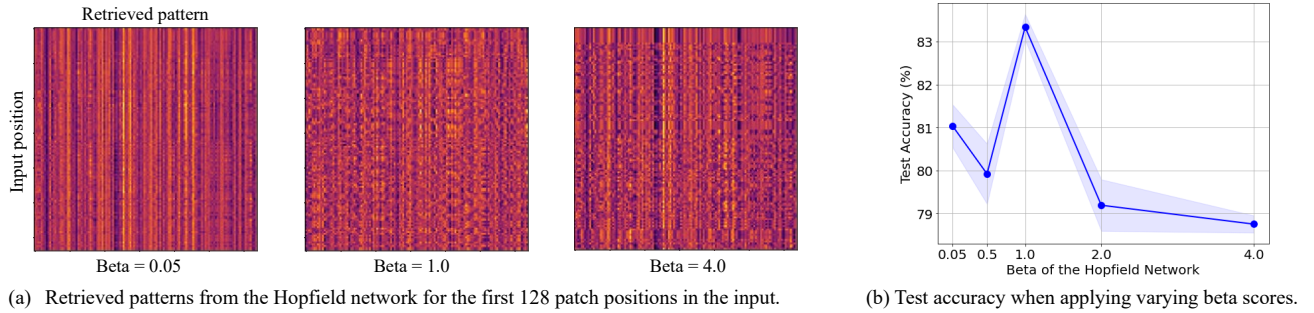


Figure 10: Varying the inverse temperature score influences the formation of the metastable states that are mixtures of patch representations. A smaller β is more likely to generate such metastable states, while a larger β leads to a stronger separation of different patterns. However, the results showed that a larger β could also lead to local minima, where input patterns were reconstructed to the same pattern.